HHS Public Access

Author manuscript

Biomaterials. Author manuscript; available in PMC 2022 January 01.

Published in final edited form as:

Biomaterials. 2021 January ; 264: 120405. doi:10.1016/j.biomaterials.2020.120405.

Development of Systemic Immune Dysregulation in a Rat Trauma Model of Biomaterial-Associated Infection

Casey E. Vantucci[*,2,3], **Hyunhee Ahn**[*,1,4], **Travis Fulton**[1,4], **Mara L. Schenker**[4,5], **Pallab Pradhan**[3], **Levi B. Wood**[2,3,6], **Robert E. Guldberg**[7], **Krishnendu Roy**[2,3], **Nick J. Willett**[1,3,4]

[1]The Atlanta Veterans Affairs Medical Center Atlanta, Decatur, GA.

[2]Wallace H. Coulter Department of Biomedical Engineering, Georgia Institute of Technology and Emory University, Atlanta, GA.

[3]Parker H. Petit Institute for Bioengineering and Bioscience, Georgia Institute of Technology, Atlanta, GA.

[4]Department of Orthopaedics, Emory University, Atlanta, GA.

[5]Grady Memorial Hospital, Atlanta, GA.

[6]George W. Woodruff School of Mechanical Engineering, Georgia Institute of Technology, Atlanta, GA.

[7]Knight Campus for Accelerating Scientific Impact, University of Oregon, Eugene, OR.

Abstract

Orthopedic biomaterial-associated infections remain a major clinical challenge, with *Staphylococcus aureus* being the most common pathogen. *S. aureus* biofilm formation enhances immune evasion and antibiotic resistance, resulting in a local, indolent infection that can persist long-term without symptoms before eventual hardware failure, bone non-union, or sepsis. Immune modulation is an emerging strategy to combat host immune evasion by S. *aureus*. However, most

Corresponding Authors: Nick J. Willett, PhD, Emory University School of Medicine, Division of Orthopaedics, 5A125 1670 Clairmont Rd. Decatur, GA, 30033; Phone: 404-385-4168; nick.willett@emory.edu; **Krishnendu Roy, PhD**, Georgia Institute of Technology and Emory University, Wallace H. Coulter Department of Biomedical Engineering, 950 Atlantic Dr. NW Atlanta, GA, 30332; Phone: 404-385-6166; krishnendu.roy@bme.gatech.edu.

[*]**Author contributions:**denotes equal contributions. CEV, HA, PP, and NJW performed experiments. CEV and HA performed the data analysis. CEV, HA, MLS, PP, LBW, REG, KR, and NJW contributed to data interpretation. HA, MLS, KR, and NJW designed experiments. CEV and HA wrote the manuscript. CEV, HA, MLS, PP, LBW, REG, KR, and NJW helped make critical revisions to the manuscript. All authors have read and approved the final manuscript.

Credit Author Statement

CEV: Methodology, Formal Analysis, investigation, Writing – Original Draft, Writing – Review & Editing, Visualization; HA: Conceptualization, Methodology, Formal Analysis, Investigation, Writing – Original Draft, Visualization; TF: Formal Analysis, Investigation, Writing – Review & Editing, Visualization. MLS: Conceptualization, Methodology, Writing – Review & Editing. PP: Methodology, Writing – Review and Editing. LBW: Conceptualization, Methodology, Writing – Editing & Review, Visualization. REG: Conceptualization, Writing – Editing & Review, Supervision. KR: Conceptualization, Methodology, Writing – Editing & Review, Supervision. NJW: Conceptualization, Methodology, Resources, Writing – Review & Editing, Supervision.

Declaration of interests

☒ The authors declare that they have no known competing financial interests or personal relationships that could have appeared to influence the work reported in this paper.

immune modulation strategies are focused on local immune responses at the site of infection, with little emphasis on understanding the infection-induced and orthopedic-related systemic immune responses of the host, and their role in local infection clearance and tissue regeneration. This study utilized a rat bone defect model to investigate how implant-associated infection affects the systemic immune response. Long-term systemic immune dysregulation was observed with a significant systemic decrease in T cells and a concomitant increase in immunosuppressive myeloid-derived suppressor cells (MDSCs) compared to non-infected controls. Further, the control group exhibited a regulated and coordinated systemic cytokine response, which was absent in the infection group. Multivariate analysis revealed high levels of MDSCs to be most correlated with the infection group, while high levels of T cells were most correlated with the control group. Locally, the infection group had attenuated macrophage infiltration and increased levels of MDSCs in the local soft tissue compared to non-infected controls. These data reveal the widespread impacts of an orthopedic infection on both the local and the systemic immune responses, uncovering promising targets for diagnostics and immunotherapies that could optimize treatment strategies and ultimately improve patient outcomes.

Keywords

severe trauma; orthopedic infection; immune dysregulation; myeloid-derived suppressor cells; *Staphylococcus aureus*

INTRODUCTION

Orthopedic implant-associated infections, such as those following joint replacement or trauma surgery, represent a significant clinical challenge, costing up to an additional $150,000 per patient in the United States (1). For most orthopedic patients, implant-associated infections occur at a rate of about 1–5%; however, for certain higher-risk groups, including patients with open fractures or those requiring revision surgery of failed prosthetic joints, infection rates are drastically increased, affecting around 20% of patients (2–5). Orthopedic infections are the most common complication with procedures involving orthopedic implants and hardware (6). In addition, these infections are challenging to treat and can result in impaired bone healing and hardware or implant failure, requiring subsequent interventions, extended rehabilitation times, long-term antibiotics, and overall increased total health and societal costs (7).

Orthopedic hardware and biomaterial implants can provide necessary fracture stability, support tissue regeneration, and replace damaged or diseased joints; however, these materials also provide an ideal environment for bacteria to colonize and grow. *Staphylococcus aureus* is the most frequent orthopedic-implant associated organism, found in 34% of orthopedic infections (8). *S. aureus* can adhere to biomaterial implant surfaces within hours and form a complex structure surrounded by self-generated extracellular polymeric substance matrix, called a biofilm, which is comprised of proteins, polysaccharides, lipids, and nucleic acids (9). These biofilms have an extensive secretome, releasing proteins that include hemolysins, leukocidins, nucleases, and endotoxins which lyse or inactivate innate and adaptive immune cells, alter immune cell signaling pathways

and cytokine expression, and prevent complement activation, all ultimately inhibiting and depressing host immunity (10). The specialized microenvironment created by the biofilm also results in decreased metabolism and growth rate, altered nutrient requirements, and mutability, all contributing to extreme antibiotic resistance where biofilms can survive antibiotic exposures up to 1000 times greater than planktonic *S. aureus* (10). Additionally, biofilm impairment of host immunity and resistance to antimicrobial factors can enable *S. aureus* invasion and colonization of the canalicular network within the bone, making the infection even more challenging to treat as bacterial cells become inaccessible deep within these networks (10,11). Successful survival of the bacteria in the host and the subsequent release of bacterial factors in combination with host immune responses can result in eventual bone lysis with decreased osteoblast viability and increased bone resorption (12,13).

The ability of biomaterial-associated infections to form biofilms that can evade the immune response and that can colonize within the canalicular networks may result in a local, indolent and chronic infection, meaning that the infection is slow-growing and does not pose an immediate threat to the patient or initially result in outward systemic symptoms, such as a fever or pain and swelling of the joint (14). However, although the patient is not in any immediate danger, these types of chronic indolent infections can persist for months or even years without symptoms and are often only discovered after catastrophic joint or hardware failure, non-union of the bone in the case of traumatic injuries, or even bacteremia and sepsis (15). Current treatment for chronic orthopedic infections requires surgical removal and debridement of the biofilm and infected tissue, removal of the implant or hardware, and eventual replacement and re-implantation of a new implant or prosthesis (16). Additionally, patients are put on an intense antibiotic regimen that can last weeks or even months in an attempt to eliminate any residual colonies or bacteria that may have detached from the biofilm during surgery and debridement (13). However, despite these aggressive measures, the rate of joint re-infections is still around 10%, with some studies observing re-infection rates above 50% (13). Because of this, current research is focused on addressing orthopedic infections through various methods including polymeric carriers for targeted delivery of antibiotics or antimicrobial peptides, implant materials with anti-infection and antimicrobial properties, and local immune modulation (2,18).

Strategies aiming to modulate the local immune environment to treat orthopedic implant-associated infections are thought to have some parallels to local immune modulation strategies of the immunosuppressive tumor environment. In particular, an ineffective T cell response and an increase in immunosuppressive cell types. such as myeloid-derived suppressor cells (MDSCs) and T regulatory cells (Tregs), are hallmarks of the immune-compromised local environment of implant-related bone infections, similar to the tumor microenvironment (19,20). Immune therapies targeting various immune cells, including T cells and MDSCs, have shown promise in cancer immunotherapy for reducing tumor burden and increasing patient survival, and have the potential to be repurposed for other diseases involving immunosuppression, such as chronic infections (13). However, despite extensive work understanding the local infection immune microenvironment and the mechanisms of immune evasion by *S. aureus*, very little focus has been placed on understanding the systemic immune response and its role in host immunity, infection clearance, and bone regeneration in the case of traumatic injury. Recent biomaterials work has highlighted the

relationship between the systemic and local immune environments and the importance of systemic immunity. In particular, systemic immune homeostasis is shown to be altered by local biomaterial scaffolds for tissue regeneration (21), and more interestingly, systemic immunity is required for successful anti-tumor immune therapy, suggesting that local immune modulation alone without systemic modulation may not be sufficient for successful intervention (22). Based on the links between bone, orthopedic infections, and the immune system, as well as the relationship between the local and systemic immune environments, the systemic immune environment may be crucial for successful immune modulation to treat chronic infections.

Host immunity is essential for bacterial clearance and appropriate and regulated healing; however, the role of the systemic immune response in particular is not well understood and has not been a major focus for addressing orthopedic implant-associated infections thus far. Therefore, in this study, the objective was to characterize the systemic immune response to an orthopedic biomaterial-associated infection following severe trauma. We hypothesized that a local, indolent infection combined with trauma would not only lead to local changes in the immune environment, but also to systemic immune dysregulation and immunosuppression. A better understanding of the systemic immune response to an orthopedic biomaterial-associated infection could provide biomarkers for early identification of chronic infection patients prior to catastrophic events such as hardware failure, bone non-union, and sepsis and could identify potential immunomodulatory targets, optimizing therapeutic interventions and improving outcomes for these patients.

METHODS

Micro-organism preparation

A bio-luminescent strain of *Staphylococcus aureus* (Xen29, PerkinElmer, Waltham, MA) was cultured in Luria Bertani (LB) medium containing 200 μg/ml kanamycin at 37°C, under aerobic conditions while agitated at 200 rpm for ~2–3 hours.

Surgical procedures

All animal care and experimental procedures were approved by the Veterans Affairs Institutional Animal Care and Use Committee (IACUC) and carried out according to the guidelines. Unilateral 2.5mm femoral segmental defects were created in 21-week old female Sprague-Dawley rats (Charles River Labs) in a similar manner to previous segmental defects (23). Briefly, an anterolateral incision was made along the length of the femur and the vastus lateralis was split with blunt dissection. A modular fixation plate was affixed to the femur using miniature screws (JI Morris Co., Southbridge, MA, USA). The 2.5mm segmental defect was then created in the diaphysis using a Gigli wire saw (RISystem, Davos, Switzerland). A collagen sponge with bacteria inoculum, *S. aureus* at 10^7 CFU (infection, n=6 due to one rat euthanized on Day 2) or without bacteria inoculum (control, n=7) was placed in the defect (Figure 1A). The fascia was then sutured closed with absorbable 4–0 sutures, and the skin was closed with wound clips. Buprenorphine SR (0.03 mg/kg; 1 ml/kg) was used as an analgesic and applied via subcutaneous injection. Antibiotics were not administered based on current clinical standard of care that exclude long-term antibiotic

treatment for closed fractures (24). Body temperature and weight were recorded prior to surgery and monitored longitudinally after surgery at days 1, 3, 7, 14, 28, and 56.

Microbiological analysis

Bacterial metabolic activity was monitored *in vivo* using serial bioluminescent (BL) scanning (In-Vivo Xtreme, Bruker Corp., Billerica, MA, USA) at days 3, 7, 14, and 56. X-rays were taken together with BL scanning as reference images. Bacterial contamination was also confirmed at 8 weeks post-surgery via wound swab culture. Presence of Xen29 can be distinguished from background levels around ~1.80e10 CFU *in* vitro in optimal growth conditions (LB media, 37C). (Supplementary Figure 1).

Immune Characterization

Circulating cellular analysis—Whole blood was collected via the rat tail vein longitudinally at days 0 (baseline), 1, 3, 7, 14, 28, and 56 for flow cytometry analysis. Red blood cells were lysed using 1X RBC lysis buffer (eBioscience) according to the manufacturer's instructions. Cells were then fixed using Cytofix fixation buffer (BD) and resuspended in buffer containing 2% fetal bovine serum (FBS) in 1X PBS and stored at 4˚C until stained. Prior to staining, cells were blocked with purified anti-rat CD32 (BD) to prevent nonspecific binding. Cells were then stained for various immune cell populations, including T cells (CD3+) and T cell subsets (CD4+, CD8+, and FoxP3+), B cells (B220+), and MDSCs (His48+CD11b+) with specific anti-rat antibodies (eBioscience). Sample data were collected using a BD Accuri C6 flow cytometer and analyzed with FlowJo. Gates were positioned with less than 1% noise allowed based on fluorescent minus one (FMO) controls.

Tissue cellular analysis—At the week 8 endpoint, tissues were harvested for immune cell population analyses including: local soft tissue adjacent to the defect site, the spleen, and bone marrow from both the contralateral leg and the tibia from the injured leg. Cells were stained for various immune cell populations, including B cells (B220+), MDSCs (His48+CD11b+), tissue macrophages (His36+), and hematopoietic stem cells (HSCs, CD45+CD90-) in the bone marrow only with specific anti-rat antibodies (eBioscience). Staining and analysis procedures were the same as for the circulating cellular analyses.

Cytokine and chemokine analysis—Serum was isolated from whole blood at the same timepoints as the circulating cellular analysis by allowing the blood to clot overnight at 4°C. Samples were then centrifuged at 1500g for 10 min and the supernatant was collected and stored at −80°C until analysis. Multiplexed chemokine and cytokine analysis was performed using Milliplex MAP Rat Cytokine/Chemokine Magnetic kit (Millipore Sigma) and analyzed using a MAGPIX Luminex instrument (Luminex). Median fluorescent intensity values with the background subtracted were used for multivariate analyses.

Micro-computed tomography

Bone formation from the injured site was quantitatively assessed using micro-computed tomography (uCT) scans (Micro-CT40, Scanco Medical, Bruttisellen, Switzerland) at 8 weeks. Samples were scanned with a 20 μm voxel size at a voltage of 55 kVp and a current of 145 μA. The bone volume was quantified only from the defect region, and new bone

formation was evaluated by application of a global threshold corresponding to 50% of the cortical bone density (386 mg hydroxyapatite/cm^3).

Histological analysis

After euthanasia at 8 weeks post-surgery, upper hindlimb explants were harvested and fixed with 10% neutral buffered formalin (10% NBF) for 3 days and then stored in 70% ethanol until processing. To observe bone structure, decalcified bone samples were embedded in paraffin and cut using a microtome (Leica Microsystems, Wetzlar, Germany) to an average thickness of 10 μm. Deparaffinized slides were then stained with Hematoxylin &Eosin (H&E) staining to demonstrate new bone formation. Images were obtained with an Axio Observer Z1 microscope (Carl Zeiss, Oberkochen, Germany) and captured using the AxioVision software (Carl Zeiss, Oberkochen, Germany).

Statistical analysis

Statistical significance for quantitative results was assessed using appropriate parametric or non-parametric tests. For data that met the assumptions, an unpaired Student's t-test, one-way analysis of variance (ANOVA), or two-way ANOVA with repeated measures were used. Multiple comparisons were made using Sidak's multiple comparisons test, and significance was determined by p values less than 0.05. For data that did not meet the assumptions for parametric tests, the Mann-Whitney test was used. Additionally, restricted maximum likelihood estimation (REML), a method for mixed effects modeling, was used for repeated measures analysis of the circulating immune cell data. This test is recommended for multiple comparisons of repeated measures data when some values are missing. Numeric values are presented as the mean ± SEM. All statistical analysis was performed using GraphPad Prism 8.0 software (GraphPad, La Jolla, CA, USA).

Luminex data was further analyzed by partial least square discriminate analysis (PLSDA) in MATLAB (Mathworks) using the partial least squares algorithm by Cleiton Nunes (Mathworks File Exchange) following z-scoring to normalize the data. PLSDA analysis reduces the dimensionality of the input variables into a set of latent variables (LVs) that maximally separate discrete groups (i.e. infection versus control). Latent variables are composed of profiles of the input variables that represent their relative contributions to the latent variables, and thus the separation between the groups. Monte Carlo sub-sampling with 1,000 iterations was done to determine the standard deviation for each of the individual signals in the LV loading plot. For each iteration, all but one of the samples were randomly sampled and a new PLSDA model was determined. Sign reversals were corrected by multiplying each sub-sampled LV by the sign of the scalar product of the new LV and the corresponding LV from the total model. The mean and standard deviation were then computed for each signal across all iterations. Lastly, heat maps of the z-scored data for all cytokine values were generated.

RESULTS

Establishment of a local infection associated with a biomaterial implant

Temperature and weight—Body temperature and weight change were measured longitudinally after surgery. Neither body temperature nor weight were significantly different between the infection animals and the non-infected, control animals at any time point or overall (Figure 1B). Throughout the 56-day time period, infection animals showed normal weight gain and did not have elevated body temperatures compared to the control animals, indicating that the infection remained local and did not spread systemically.

Bioluminescent scans and endpoint evaluation of infection—Bioluminescent scans indicating metabolic activity of the bacteria were assessed following inoculation (Figure 1C). Bioluminescent signal was present in infection animals as early as Day 3 post-surgery and up until Day 7; however, it should be noted that bioluminescence is indicative of metabolic activity of the cells, not necessarily cell presence. No signal was observed in the control animals at any time point. Despite the absence of bioluminescent signal beyond Day 7 *in vivo*, wound swab culture conducted at the Day 56 endpoint confirmed the presence of bacteria in the infection animals (Figure 1D, Supplementary Figure 2). Additionally, in another animal cohort, wound swab cultures at both 8 and 10 weeks exhibited bioluminescent signal, demonstrating long-term persistence of the infection (Supplementary Figure 3). No bacterial growth was observed in culture following wound swab of the non-infected, control animals (Figure 1D, Supplementary Figure 2). Further, inspection of the thighs of euthanized infection animals showed gray, necrotic soft tissue and purulence around the implant hardware, which was not present in the control animals (Figure 1E).

Local infection alters local and systemic immune profiles

Systemic immune cell populations—Circulating immune cell populations of both immune effector cells and immunosuppressive cells were evaluated using flow cytometry and revealed differences in the systemic immune response in the infection versus control animals (Figure 2). Immune effector cells evaluated included both T and B cells (Figure 2A), as well as the helper T cell and cytotoxic T cell subsets (Figure 2B). Immunosuppressive cells evaluated (Figure 2B,C) included MDSCs and Tregs, an immunoregulatory T cell subset. At Day 1 post-injury, there was a significant decrease in circulating T cells, helper T cells, and cytotoxic T cells in both the infection and control groups compared to the baseline. Over time, T cell populations, including helper T cell and cytotoxic T cell subsets, gradually increased in both groups until Day 28. However, while the T cell populations in the control group increased back to baseline levels, the T cell populations in the infection group remained significantly lower overall compared to baseline and the control group.

For B cells, there was a similar decrease in cell numbers in the control group, whereas there was an increase in B cells in the infection group, which peaked at Day 7. Following Day 7, B cells in the infection group continue to decline, whereas B cells in the control group remained relatively constant. For the immunosuppressive cell types, at Day 1 post-injury, there was a significant systemic increase in MDSCs in both the infection and control groups compared to baseline with the highest peak level of MDSCs in the infection group. MDSCs

in both groups gradually decreased until Day 28; however, MDSCs in the infection group were overall elevated compared to the control group. Tregs showed no significant differences between the groups. Overall, there were decreases in T cells, helper T cells, and cytotoxic T cells (p=0.06) and increases in immunosuppressive MDSCs in the infection group compared to the control group.

Tissue immune cell populations—At the Day 56 endpoint, tissue was collected from the spleen, the soft tissue adjacent to the defect, and the bone marrow in the injured and contralateral legs. Similar to systemic cellular analysis, immunosuppressive MDSCs were elevated in infection animals compared to control animals in both local soft tissue and the bone marrow, but not in the spleen (Figure 3). Macrophages, another immune effector cell type, were found to be decreased in the infection group in the local soft tissue (adjacent to the bone defect), the spleen, and the bone marrow compared to the control group. Additionally, B cells in the local soft tissue and the spleen were found to be lower in the infection group compared to the control group, consistent with Day 56 circulating B cell levels which were also lower in the infection group. Analysis of hematopoietic stem cells in the bone marrow revealed a slight decrease in the infection animals compared to the control animals but were not significantly different (Figure 3C,D). Despite a decrease in circulating T cells in infection animals compared to the control animals, there were no significant differences in T cell populations in any of the tissues.

Cytokine and chemokine profiles—Serum was analyzed for changes in systemic cytokine and chemokine levels over time. The cytokine and chemokine data were z-scored (mean subtracted and normalized to standard deviation for each cytokine) and plotted on a heat map (Figure 4A). The control group revealed coordinated up-regulation of specific cytokines at Day 1, Day 7, and Day 14, which appeared to resolve by Day 28. Qualitatively, the coordinated regulation of cytokine and chemokine levels was not observed in the infection group. Quantitatively, there were no significant differences in baseline levels between the groups for any of the cytokines (Supplementary Figure 4A). At Day 1, epidermal growth factor (EGF), macrophage chemoattractant protein-1 (MCP-1), and LIX were significantly upregulated in the control group compared to the infection group (Figure 4B). All of these factors are involved in cell migration and recruitment, cell survival, and differentiation. Additionally, IL-2, a cytokine important for T cell function, was upregulated in the infection group compared to the control group at Day 1 (Figure 4B). No other cytokines were significantly different between groups at Day 1 (Supplementary Figure 4B). On Day 3, RANTES, a chemokine important for leukocyte recruitment, was significantly upregulated in the control group compared to the infection group, and IL-10, a general immunosuppressive cytokine, was significantly elevated in the infection group compared to the control group (Figure 4C). No other cytokines were significantly different between groups at Day 3 (Supplementary Figure 4C). By Day 7 and 14, a large number of both pro- and anti-inflammatory cytokines were all significantly upregulated in the control group compared to the infection group (Supplementary Figure 4D,E). The inflammation in the control group resolved between Day 14 and Day 28, with cytokine and chemokine levels returning to baseline levels. At Day 28, there were no significant differences between groups for any of the cytokines (Supplementary Figure 4F); however, by Day 56, several cytokines

including IL-4, IL-12p70, IL-17A, and TNFa were all upregulated in the infection group compared to the control group (Supplementary Figure 4G).

Overall systemic immune characterization—To investigate the overall contributors that distinguished the infection group from the non-infected, control group, partial least squares discriminant analysis (PLSDA) was conducted on data aggregated from all timepoints post-injury, including cellular and chemokine data (Figure 5A). This analysis revealed a significant separation of the two groups according to latent variable 1 (LV1) (Figure 5B). The LV1 loading plot shows the major contributors to positive LV1 values (control group) and negative LV1 values (infection group) (Figure 5C). The main contributors to the control group were T cells and the T cell effector subsets, including helper T cells and cytotoxic T cells. Contributing most to the infection group were the immunosuppressive MDSCs, B cells, and the cytokine IL-10, which has typically been considered immunosuppressive in the context of trauma and sepsis (25,26). Plotting the same datapoints from the PLSDA plot in Figure 5A with only the infection group data points (Figure 5D) or only the control group data points (Figure 5E) highlights that there is a separation based on response time regardless of infection. The early response (Day 1 and Day 3), the intermediate response (Day 7 and Day 14), and the late response (Day 28 and Day 56) of the cells and cytokines all cluster separately on the PLSDA plot for the infection group and the control group. The infection group clusters are significantly separated only on the LV1 axis (Supplementary Figure 5A,B), where the top factors correlated with separation are cells, including T cells, MDSCs, and B cells, but not cytokines (Supplementary Figure 5E). On the other hand, the control group clusters are significantly separated based on both the LV1 and LV2 axes (Supplementary Figure 5C,D). The intermediate response (Day 7 and Day 14) for the control group shows significant separation from the early and late responses along the LV2 axis, where the top factors correlated with separation are cytokines (Supplementary Figure 5F), consistent with the large upregulation of cytokines observed in the heat map for the control group at Days 7 and 14. The late response (Day 28 and Day 56) for the control group shows significant separation from the early and intermediate responses along the LV1 axis, where the top factors correlated with separation are again cells, but not cytokines (Supplementary Figure 2E). These data highlight whether cells or cytokines are the major drivers of the systemic immune response at different timepoints in the control and infection groups.

Bone regeneration and histological analysis

At the Day 56 endpoint, bone explants were harvested for micro-computed tomography (uCT) and histological evaluation. There were no significant differences in new bone formation between the control and infection animals, although the control group did have higher peak bone formation (Figure 6A). Further, histological analysis revealed an abnormal ectopic periosteal response in the bone from the infection animals, with aberrant and scattered periosteal bone formation (Figure 6B). Bone in the non-infected, control group showed new bone formation at the defect region according to hematoxylin and eosin staining.

DISCUSSION

Despite advancements in surgical procedures and antimicrobial regimens, orthopedic biomaterial-associated infections remain a challenging clinical problem; failure rates remain high and there has been little to no improvement in infection-related patient outcomes over the past several decades (27). Complicating the matter for fracture-associated infections, there is currently no consensus on diagnostic criteria and therefore very few protocols for diagnosis and treatment (28). Characterization of the systemic immune response to an orthopedic biomaterial-associated infection could allow for better identification of biomarkers to identify at-risk patients and for immunotherapeutic targets that could improve local therapeutic interventions and overall outcomes for these patients. In this manuscript we utilized a rat trauma model with a biomaterial-associated infection to analyze the long-term immune response to a local, indolent orthopedic infection. While this model does not investigate the complexities of bacteria-scaffold interactions, this model still mimics clinical aspects of a chronic implant-associated bone infection, including no systemic symptoms (weight loss, fever, etc.) and eventual detection of the infection by hardware failure and/or nonunion of the defect. Pilot studies exhibited hardware failure at higher CFU; however, the dose was reduced for this study to prevent hardware failure during the time course of the experiment. One limitation of this study is the lack of longitudinal local immune analysis and evaluation of specific antibody responses against *S. aureus.* However, both of these aspects of the immune response to infection have been extensively studied (13,27), whereas this study focuses on the under-investigated systemic immune response to a local infection.

In the presence of orthopedic infection in a rat trauma model, depressed systemic immunity was observed compared to trauma without infection. This change was most notable with increased immunosuppressive MDSCs and decreased T cells, including the helper T cell and cytotoxic T cell subsets. MDSCs are a heterogeneous and immature myeloid-derived cell population characterized by their immunosuppressive function, and they expand during conditions of acute and chronic inflammation, including trauma, sepsis, infection, and cancer (29–32). MDSCs utilize various mechanistic pathways to suppress the activity of immune effector cells, including the production of immunosuppressive cytokines such as IL-10 and TGF-β, release of reactive oxygen and reactive nitrogen species (ROS/RNS), and stimulation of immunosuppressive Tregs. Additionally, MDSCs can suppress T cell function through arginase-1 activity that depletes L-arginine, an essential amino acid required for T-cell receptor (TCR) signaling (33,34). Prevention of T cell activation inhibits one of the major adaptive immune response mechanisms to pathogen-associated molecular patterns (PAMPs) and danger-associated molecular patterns (DAMPs), which are molecular motifs associated with infection and damaged or stressed tissue (13). Additionally, in the context of infection and cancer, MDSCs are known for suppressing cytotoxic T cell and Natural Killer (NK) cell function, preventing immune responses to bacteria and tumors (32,35). The resulting immunosuppression allows bacteria to evade recognition and clearance by the immune system, contributing to bacterial persistence and chronicity of local, indolent infections (13).

In this study, B cells in the blood of the infection group initially increased to levels higher than the non-infected, control group, peaking around Day 7. Following Day 7, B cell levels

in the infection group notably decline, whereas B cell levels in the control group remain relatively constant and are not significantly different from baseline levels from Day 3 onward. *S. aureus* is known to modulate the B cell response by triggering B cell-mediated immune tolerance through the virulence factor Staphylococcal Protein A (SpA) (36). SpA stimulates B cell expansion and subsequently activation-induced B cell death due to the absence of co-stimulation (37). Additionally, SpA is known to manipulate B cell affinity maturation, inhibit long-lived plasma cells, and induce immune tolerogenic IL-10 producing B cells, thus limiting the host response, preventing memory formation, and increasing the risk for chronic and recurring infection (38,39). This mechanism is consistent with our observation of the cellular immune data showing a continual decline in B cells in the infection group after a peak at Day 7 and with the cytokine data showing a significant increase in IL-10 in the infection group compared to the control group.

While there were overall differences in systemic cellular immunity between the infection and control groups and between each group and their baseline levels, there were few significant differences between groups at individual timepoints. The lack of individual differences in cell populations may in part be due to the complexity of the interactions between the different mediators. Additionally, as a limitation of this study, we did not conduct functional analyses of the various immune cell populations or investigate heterogeneity within subsets of cell types, which may highlight further and more significant differences in these populations.

Cellular analyses of local tissues showed similar results as the systemic analysis with upregulation of immunosuppressive MDSCs in the local soft tissue surrounding the defect, as well as in the bone marrow, compared to the control group. Conversely, macrophages were elevated in the non-infected, control group in the bone marrow and the spleen as well as dramatically in the local soft tissue when compared to the infection group. This is consistent with *S. aureus* biofilm formation which is known to alter the local environment in order to impair immune effector cell function, such as macrophages, while enhancing the expansion of immunosuppressive MDSCs (13). Therefore, in the presence of infection, the immunosuppressive immune environment can prevent infiltration of macrophages, whereas, the lack of infection in the control group can permit extensive macrophage infiltration into the defect site. Due to an emphasis on the systemic immune response, one limitation of this study was a lack of characterization of macrophage phenotype infiltrating into the defect region. Future work to better understand the interactions between both the local and systemic environments could be essential for identifying appropriate immunomodulatory targets to enhance bacterial clearance and improve tissue regeneration.

Overall analysis of circulating cytokine levels revealed a regulated and coordinated immune response with resolution of inflammation sometime between Day 14 and Day 28 in the non-infected, control group. In contrast, the infection group lacked a similar coordinated response at any timepoint or with any set of cytokines compared to the control group. Looking at significant cytokine differences between groups prior to Day 7, there was early upregulation of cytokines involved in cell recruitment, proliferation, and survival in the control group compared to the infection group, including EGF, MCP-1 (also known as CCL2), and LIX (also known as CXCL5) at Day 1, and RANTES (also known as CCL5) at

Day 3. Under inflammatory conditions, EGF is a potent inducer of angiogenesis and bone growth, significantly upregulating secretion of vascular endothelial growth factor (VEGF) and bone morphogenetic protein-2 (BMP-2), an osteoinductive growth factor (40). MCP-1 has also been shown to be a key cytokine involved in both inflammation and bone remodeling, in part by promoting neutrophil migration, macrophage infiltration, and angiogenesis (41). Similarly, LIX and RANTES are known for their chemotactic and pro-inflammatory properties that have both been associated with the necessary early inflammatory phase during the fracture repair process (42,43). In the infection group however, immunosuppressive IL-10 was upregulated as early as Day 3 compared to the control animals, which may have subsequently inhibited a coordinated and regulated inflammatory response. This increase in IL-10 is supported by a sharp increase in MDSCs, which are known to release IL-10, as early as Day 1 in the infection group. At Days 7 and 14, multiple inflammatory cytokines were upregulated in the control group compared to the infection group (Supplementary Figures 1D,E), which all resolved back to baseline levels by Day 28. The inflammatory response after fracture repair is a highly coordinated process that is required for successful repair and regeneration of severe injuries in order to recruit appropriate cells and clear necrotic tissue (44). However, a similar inflammatory response was not seen in the infection group. Many of the cytokines that were elevated in a coordinated, temporal process in the control animals remained at low levels in the infection animals, particularly in the first two weeks. At Day 56, several cytokines, including IL-4, IL12p70, IL-17A, and TNFa, were upregulated in the infection group compared to the control group, highlighting that the dysregulated cytokine response continues long-term in the infection group.

In addition to looking individually at cell populations and cytokine levels, we also conducted multivariate analyses that can account for interaction effects to allow us to better understand the role of systemic factors in response to an orthopedic biomaterial-associated infection. The PLSDA loading plot showed mainly cell types, not cytokines, as the top factors associated with each group. The non-infected, control group was most positively associated with T cells (CD3 T cells), including the helper T cell (CD4 T cells) and cytotoxic T cell (CD8 T cells) subsets. Functioning immune effector cells are necessary for a coordinated and regulated immune response to trauma. In particular, an absence of T cells following fracture has been shown to result in disrupted bone mineralization and decreased bone regeneration. This effect has been associated with the role of T cells in normal collagen deposition during the early stages of callus formation (45). In addition, systemic dysregulation of helper T cells has been associated with increased risk for multiple organ failure and death in trauma and burn patients (46), again highlighting the importance of T cells and their subsets for appropriate healing. In contrast, the top factors most associated with the infection group included MDSCs, B cells, and IL-10. Immunosuppressive MDSCs, which are known to release the cytokine IL-10 and expand following bacterial infection, can be a sign of a dysregulated immune response (32). In addition, *S. aureus* is also known to modulate the B cell response by enhancing the population of immune tolerogenic IL-10 producing B cells (36,38).

Interestingly, the systemic immune dysregulation and immunosuppression evidenced in the infection group has been reported before in other diseases and conditions, including sepsis

and severe musculoskeletal trauma (47). In both trauma and sepsis, there is a massive early innate immune response, resulting in over-production of pro-inflammatory mediators (e.g. Type I Interferons, IL-1, IL-6, IL-8, TNFa) and systemic activation of innate immune cells (44,48). Concurrently, the body's defense mechanisms trigger a compensatory anti-inflammatory response through systemic up-regulation of immunosuppressive mediators (e.g. IL-10, TGF-b) and cells, such as MDSCs and Tregs (30,49–52). A balance between the two responses leads to restoration of systemic immune homeostasis typically within the first week or two and is associated with successful healing and regeneration, similar to what we see in the control group in our rat infection model. However, when the anti-inflammatory response overwhelms the initial inflammatory response, systemic immune dysregulation develops, marked by increases in immunosuppressive mediators, decreases in immune effector cell numbers and function, and an overall decrease in host immunity (49,53). In all of the cases discussed – implant-associated orthopedic infection, sepsis, and severe musculoskeletal trauma – widespread systemic immunosuppression results after overactivation of the immune system either from bacterial infection or from damaged host tissue. Therefore, in any situation resulting in similar immune overactivation, systemic immune dysregulation could arise and may impact patient outcomes.

Creation of a local, indolent infection with *S.* aureus-soaked collagen sponges implanted in the defect site was confirmed by normal weight gain and temperature, bacterial presence after endpoint wound swab culture, and longitudinal bioluminescent imaging, although bioluminescent signaling dropped below the threshold of detection past Day 7. Following biofilm formation, *S. aureus* is known to undergo significant metabolic changes, including down-regulation of transcription, translation, and aerobic processes, resulting in an overall decrease in metabolic activity of the active infection. For example, physiologically dormant "persister" cells are protected by the biofilm matrix and thought to grow at significantly slower rates than metabolically active planktonic cultures (54–56). Reductions in bioluminescent signal despite no significant decrease in bacterial load has also been observed in several other related mouse osteomyelitis models (57–59). Therefore, the absence of bioluminescent signal past Day 7 is not indicative of infection clearance but likely indicative of biofilm formation and decreased metabolic activity, resulting in bioluminescent signal that falls below the limits of detection of our instrumentation (Supplementary Figure 1).

In addition to the unexpected lack of bioluminescent signal past Day 7 in the infection group, we also observed no significant differences in bone regeneration volumes between groups, despite the sub-critical size of the bone defect. The non-infected, control group bone defects contained a collagen sponge, which is clinically approved for use in patients in conjunction with BMP-2, an osteoinductive growth factor. While this study did not utilize BMP-2, collagen based-materials are attractive options for bone substitutes because collagen is the main organic polymer in bone matrix. Additionally, collagen scaffolds have had success in tissue engineering and wound healing applications to facilitate cell growth and differentiation, promote intrinsic vascularization, and provide an infrastructure for osteogenesis and chondrogenesis by supporting cell invasion (60). There are multiple collagen-based composite bone substitutes used clinically for bone applications, including Cerasorb Ortho Foam, a collagen-tricalcium phosphate composite, and OssiMend, a

collagen-carbonate apatite composite (61). Despite the widespread use of collagen-based materials for bone tissue engineering, the effects of collagen sponge alone on bone healing without exogeneous factors, such as BMP-2, still remain largely unknown. However, in a recent study, *in vivo* testing of collagen sponge unexpectedly showed a negative impact on bone healing, with significantly decreased bone formation in a mouse osteotomy model compared to an empty defect (62). These results are consistent with the lack of healing observed in our study for the non-infected, control group; however, further mechanistic studies are needed to understand the potential inhibitory effects of empty collagen sponge in sub criticalsize bone defects.

The systemic immune characterization from this study identified multiple differences in immune factors as early as 3 days post-surgery that could be used to identify patients exhibiting systemic immune dysregulation following implant-associated orthopedic infection. Currently, chronic infections are often not diagnosed until weeks or months later following a catastrophic event such as hardware failure, bone non-union, or sepsis. The immune markers evaluated in this study could be used for early identification of patients exhibiting systemic immune dysregulation, which could then allow clinicians to investigate and treat patients for potential infections significantly earlier, improving outcomes and reducing healthcare costs. In addition to using early systemic immune markers to diagnose at-risk patients, this study also identified the significant driving factor of immune dysregulation to be the immunosuppressive MDSC population, offering a promising immunomodulatory target that could synergistically improve current treatment strategies, similar to cancer immunotherapy. However, further studies are still needed to better understand the role of systemic immune dysregulation and systemic immunomodulation on the local environment, including bacterial clearance and bone regeneration.

CONCLUSION

To our knowledge, this is one of the first studies investigating the systemic immune response and immune dysregulation resulting from trauma-associated orthopedic biomaterial infections. The presence of a local, indolent *S. aureus* bacterial infection resulted in widespread systemic effects, including an uncoordinated and dysregulated systemic immune response with systemic increases in immunosuppressive MDSCs and decreases in immune effector cells, including T cells. This systemic immune dysregulation and immunosuppression in combination with the local *S. aureus* infection could contribute significantly to the clinical challenges associated with infected trauma, in particular, chronic and recurring infections and poor bone regeneration. An improved understanding of the systemic immune response and its relationship with the local environment, including bacterial clearance and bone healing, could provide promising early diagnostic markers and systemic immunomodulatory targets to improve the ability to fight orthopedic biomaterial-associated infections and improve patient outcomes.

Supplementary Material

Refer to Web version on PubMed Central for supplementary material.

ACKNOWLEDGEMENTS

This research was supported partially by an ACTSI/REM Seed Grant from Emory University and Georgia Tech and Endowment to the Georgia Tech Foundation from Robert A. Milton. CEV acknowledges support by the National Science Foundation Graduate Research Fellowship under Grant No. DGE-1650044. This work was supported by an National Institutes of Health R01 grant (R01AR074960). Any opinion, findings, and conclusions or recommendations expressed in this material are those of the authors(s) and do not necessarily reflect the views of the National Science Foundation. The authors would like to thank Laura Weinstock for her assistance with the Luminex analyses. Additionally, the authors wish to acknowledge the core facilities at the Parker H. Petit Institute for Bioengineering and Bioscience at the Georgia Institute of Technology for the use of their shared equipment, services, and expertise.

REFERENCES

1. Schwarz EM, Parvizi J, Gehrke T, Aiyer A, Battenberg A, Brown SA, et al. 2018 International Consensus Meeting on Musculoskeletal Infection: Research Priorities from the General Assembly Questions. J Orthop Res. 2019 5;37(5):997–1006. [PubMed: 30977537]
2. ter Boo GJA, Grijpma DW, Moriarty TF, Richards RG, Eglin D. Antimicrobial delivery systems for local infection prophylaxis in orthopedic- and trauma surgery. Vol. 52, Biomaterials. Elsevier Ltd; 2015. p. 113–25. [PubMed: 25818418]
3. Bongers J, Jacobs AME, Smulders K, van Hellemondt GG, Goosen JHM. Reinfection and re-revision rates of 113 two-stage revisions in infected TKA. J Bone Jt Infect. 2020 May 3;5(3):137–44. [PubMed: 32566453]
4. Australian Orthopaedic Association National Joint Replacement Registry. 2019.
5. Guerra MTE, Gregio FM, Bernardi A, Castro CC de. Infection rate in adult patients with open fractures treated at the emergency hospital and at the ULBRA university hospital in Canoas, Rio Grande do Sul, Brazil. Rev Bras Ortop (English Ed. 2017 Sep;52(5):544–8.
6. Kaufman MG, Meaike JD, Izaddoost SA. Orthopedic Prosthetic Infections: Diagnosis and Orthopedic Salvage. Semin Plast Surg. 2016 May 1;30(2):66–72. [PubMed: 27152098]
7. Moriarty TF, Kuehl R, Coenye T, Metsemakers W-J, Morgenstern M, Schwarz EM, et al. Orthopaedic device-related infection: current and future interventions for improved prevention and treatment. EFORT open Rev. 2016 Apr;1(4):89–99. [PubMed: 28461934]
8. Bernard L, Lübbeke A, Stern R, Bru JP, Feron JM, Peyramond D, et al. Value of preoperative investigations in diagnosing prosthetic joint infection: retrospective cohort study and literature review. Scand J Infect Dis. 2004;36(6–7):410–6. [PubMed: 15307559]
9. Bjarnsholt T Introduction to biofilms. Biofilm Infections. 2011;1–9.
10. Ricciardi BF, Muthukrishnan G, Masters E, Ninomiya M, Lee CC, Schwarz EM. Staphylococcus aureus Evasion of Host Immunity in the Setting of Prosthetic Joint Infection: Biofilm and Beyond. Vol. 11, Current Reviews in Musculoskeletal Medicine. Humana Press Inc.; 2018. p. 389–400. [PubMed: 29987645]
11. de Mesy Bentley KL, MacDonald A, Schwarz EM, Oh I. Chronic Osteomyelitis with Staphylococcus aureus Deformation in Submicron Canaliculi of Osteocytes: A Case Report. JBJS case Connect. 2018 Jan 1;8(1):e8. [PubMed: 29443819]
12. Sanchez CJ, Ward CL, Romano DR, Hurtgen BJ, Hardy SK, Woodbury RL, et al. Staphylococcus aureus biofilms decrease osteoblast viability, inhibits osteogenic differentiation, and increases bone resorption in vitro. BMC Musculoskelet Disord. 2013;14.
13. Seebach E, Kubatzky KF. Chronic Implant-Related Bone Infections-Can Immune Modulation be a Therapeutic Strategy? Vol. 10, Frontiers in immunology. NLM (Medline); 2019. p. 1724. [PubMed: 31396229]
14. Masters EA, Trombetta RP, de Mesy Bentley KL, Boyce BF, Gill AL, Gill SR, et al. Evolving concepts in bone infection: redefining “biofilm”, “acute vs. chronic osteomyelitis”, “the immune proteome” and “local antibiotic therapy.” Bone Res. 2019 12;7(1).
15. Chapter 7. Orthopedic Infections: Basic Principles of Pathogenesis, Diagnosis, and Treatment | Current Diagnosis & Treatment in Orthopedics, 5e | AccessMedicine | McGraw-Hill Medical

[Internet]. [cited 2020 Mar 17]. Available from: https://accessmedicine-mhmedical-com.proxy.library.emory.edu/content.aspx?bookid=675&sectionid=45451713#57816196

16. Kavanagh N, Ryan EJ, Widaa A, Sexton G, Fennell J, O'Rourke S, et al. Staphylococcal osteomyelitis: Disease progression, treatment challenges, and future directions. Vol. 31, Clinical Microbiology Reviews. American Society for Microbiology; 2018.
17. Bhattacharya M, Wozniak DJ, Stoodley P, Hall-Stoodley L. Prevention and treatment of Staphylococcus aureus biofilms. Vol. 13, Expert Review of Anti-Infective Therapy. Taylor and Francis Ltd; 2015. p. 1499–516.
18. Lin X, Yang S, Lai K, Yang H, Webster TJ, Yang L. Orthopedic implant biomaterials with both osteogenic and anti-infection capacities and associated in vivo evaluation methods. Vol. 13, Nanomedicine: Nanotechnology, Biology, and Medicine. Elsevier Inc.; 2017. p. 123–42.
19. Thammavongsa V, Kim HK, Missiakas D, Schneewind O. Staphylococcal manipulation of host immune responses. Vol. 13, Nature Reviews Microbiology. Nature Publishing Group; 2015. p. 529–43. [PubMed: 26272408]
20. Heim CE, Vidlak D, Scherr TD, Kozel JA, Holzapfel M, Muirhead DE, et al. Myeloid-Derived Suppressor Cells Contribute to Staphylococcus aureus Orthopedic Biofilm Infection. J Immunol. 2014 4 15;192(8):3778–92. [PubMed: 24646737]
21. Sadtler K, Estrellas K, Allen BW, Wolf MT, Fan H, Tam AJ, et al. Developing a pro-regenerative biomaterial scaffold microenvironment requires T helper 2 cells. Science (80-). 2016 4 15;352(6283):366–70.
22. Spitzer MH, Carmi Y, Reticker-Flynn NE, Kwek SS, Madhireddy D, Martins MM, et al. Systemic Immunity Is Required for Effective Cancer Immunotherapy. Cell. 2017 1 26;168(3):487–502.e15. [PubMed: 28111070]
23. Willett NJ, Li M-TA, Uhrig BA, Boerckel JD, Huebsch N, Lundgren TL, et al. Attenuated human bone morphogenetic protein-2-mediated bone regeneration in a rat model of composite bone and muscle injury. Tissue Eng Part C Methods. 2013 4;19(4):316–25. [PubMed: 22992043]
24. Gans I, Jain A, Sirisreetreerux N, Haut ER, Hasenboehler EA. Current practice of antibiotic prophylaxis for surgical fixation of closed long bone fractures: A survey of 297 members of the Orthopaedic Trauma Association. Patient Saf Surg. 2017 1 16;11(1):2. [PubMed: 28105080]
25. Schulte W, Bernhagen J, Bucala R. Cytokines in Sepsis: Potent Immunoregulators and Potential Therapeutic Targets-An Updated View. Mediators Inflamm. 2013;2013:16.
26. Reikerås O Immune depression in musculoskeletal trauma. Vol. 59, Inflammation Research. 2010. p. 409–14. [PubMed: 20148282]
27. Muthukrishnan G, Masters EA, Daiss JL, Schwarz EM. Mechanisms of Immune Evasion and Bone Tissue Colonization That Make Staphylococcus aureus the Primary Pathogen in Osteomyelitis. Curr Osteoporos Rep. 2019;
28. Govaert GAM, Kuehl R, Atkins BL, Trampuz A, Morgenstern M, Obremskey WT, et al. Diagnosing Fracture-Related Infection. J Orthop Trauma. 2019 8;1.
29. Kumar V, Patel S, Tcyganov E, Gabrilovich DI. The Nature of Myeloid-Derived Suppressor Cells in the Tumor Microenvironment. Trends Immunol. 2016 3 1;37(3):208–20. [PubMed: 26858199]
30. Cuenca AG, Delano MJ, Kelly-Scumpia KM, Moreno C, Scumpia PO, Laface DM, et al. A paradoxical role for myeloid-derived suppressor cells in sepsis and trauma. Mol Med. 2011;17(3–4):281–92. [PubMed: 21085745]
31. Lai D, Qin C, Shu Q. Myeloid-derived suppressor cells in sepsis. Biomed Res Int. 2014;2014.
32. Ost M, Singh A, Peschel A, Mehling R, Rieber N, Hartl D. Myeloid-derived suppressor cells in bacterial infections. Vol. 6, Frontiers in Cellular and Infection Microbiology. Frontiers Media S.A.; 2016.
33. Zhu X, Pribis JP, Rodriguez PC, Morris SM, Vodovotz Y, Billiar TR, et al. The Central Role of Arginine Catabolism in T-Cell Dysfunction and Increased Susceptibility to Infection After Physical Injury. Ann Surg. 2014 1;259(1):171–8. [PubMed: 23470573]
34. Schrijver IT, Théroude C, Roger T. Myeloid derived suppressor cells sepsis. Vol. 10, Frontiers in Immunology. Frontiers Media S.A.; 2019.

35. Srivastava MK, Zhu L, Harris-White M, Kar U, Huang M, Johnson MF, et al. Myeloid Suppressor Cell Depletion Augments Antitumor Activity in Lung Cancer. Sarkar D, editor. PLoS One. 2012 7 16;7(7):e40677. [PubMed: 22815789]
36. Pauli NT, Kim HK, Falugi F, Huang M, Dulac J, Dunand CH, et al. Staphylococcus aureus infection induces protein A-mediated immune evasion in humans. J Exp Med. 2014;211(12):2331–9. [PubMed: 25348152]
37. Goodyear CS, Silverman GJ. Death by a B cell superantigen: In vivo VH-targeted apoptotic supraclonal B cell deletion by a staphylococcal toxin. J Exp Med. 2003 5 5;197(9):1125–39. [PubMed: 12719481]
38. Parcina M, Miranda-Garcia MA, Durlanik S, Ziegler S, Over B, Georg P, et al. Pathogen-Triggered Activation of Plasmacytoid Dendritic Cells Induces IL-10–Producing B Cells in Response to Staphylococcus aureus. J Immunol. 2013 2 15;190(4):1591–602. [PubMed: 23325892]
39. Keener AB, Thurlow LT, Kang S, Spidale NA, Clarke SH, Cunnion KM, et al. Staphylococcus aureus Protein A Disrupts Immunity Mediated by Long-Lived Plasma Cells. J Immunol. 2017 2 1;198(3):1263–73. [PubMed: 28031339]
40. Basal O, Atay T, Ciris İM, Baykal YB. Epidermal growth factor (EGF) promotes bone healing in surgically induced osteonecrosis of the femoral head (ONFH). Bosn J Basic Med Sci. 2018;18(4):352–60. [PubMed: 29924961]
41. Edderkaoui B Potential role of chemokines in fracture repair. Vol. 8, Frontiers in Endocrinology. Frontiers Research Foundation; 2017.
42. Bischoff DS, Zhu J-H, Makhijani NS, Yamaguchi DT. Induction of CXC chemokines in human mesenchymal stem cells by stimulation with secreted frizzled-related proteins through non-canonical Wnt signaling. World J Stem Cells. 2015;7(11):1262–12673. [PubMed: 26730270]
43. Liu YC, Kao YT, Huang WK, Lin KY, Wu SC, Hsu SC, et al. CCL5/RANTES is important for inducing osteogenesis of human mesenchymal stem cells and is regulated by dexamethasone. Biosci Trends. 2014;8(3):138–43. [PubMed: 25030847]
44. Stahel PF, Smith WR, Moore EE. Role of biological modifiers regulating the immune response after trauma. Injury. 2007;38(12):1409–22. [PubMed: 18048034]
45. Khassawna T El, Serra A, Bucher CH, Petersen A, Schlundt C, Könnecke I, et al. T lymphocytes influence the mineralization process of bone. Front Immunol. 2017 5 24;8(MAY):562. [PubMed: 28596766]
46. Miller AC, Rashid RM, Elamin EM. The “T” in Trauma: the Helper T-cell Response and the Role of Immunomodulation in Trauma and Burn Patients. Vol. 63, Journal of Trauma. 2007. p. 1407–17.
47. Vantucci CE, Roy K, Guldberg RE. Immunomodulatory strategies for immune dysregulation following severe musculoskeletal trauma. J Immunol Regen Med. 2018 9 1;2:21–35.
48. Flohe SB, Flohe S, Schade FU. Deterioration of the immune system after trauma: signals and cellular mechanisms. Innate Immun. 2008;
49. Vanzant EL, Lopez CM, Ozrazgat-Baslanti T, Ungaro R, Davis R, Cuenca AG, et al. Persistent Inflammation, Immunosuppression and Catabolism Syndrome after Severe Blunt Trauma. J Trauma Acute Care Surg. 2014;76(1):21–30. [PubMed: 24368353]
50. Kimura F, Shimizu H, Yoshidome H, Ohtsuka M, Miyazaki M. Immunosuppression following surgical and traumatic injury. Surg Today. 2010;40(9):793–808. [PubMed: 20740341]
51. Drewry AM, Samra N, Skrupky LP, Fuller BM, Compton SM, Hotchkiss RS. Persistent lymphopenia after diagnosis of sepsis predicts mortality. Shock. 2014 11;42(5):383–91. [PubMed: 25051284]
52. Hotchkiss RS, Monneret G, Payen D. Sepsis-induced immunosuppression: from cellular dysfunctions to immunotherapy. Nat Rev Immunol. 2013;13(12):862–74. [PubMed: 24232462]
53. Hawkins RB, Raymond SL, Stortz JA, Horiguchi H, Brakenridge SC, Gardner A, et al. Chronic Critical Illness and the Persistent Inflammation, Immunosuppression, and Catabolism Syndrome. Front Immunol. 2018 7 2;9.
54. Lewis K Persister Cells. Annu Rev Microbiol. 2010 10 13;64(1):357–72. [PubMed: 20528688]
55. Lister JL, Horswill AR. Staphylococcus aureus biofilms: Recent developments in biofilm dispersal. Front Cell Infect Microbiol. 2014;4(DEC).

56. Singh R, Ray P, Das A, Sharma M. Role of persisters and small-colony variants in antibiotic resistance of planktonic and biofilm-associated Staphylococcus aureus: An in vitro study. J Med Microbiol. 2009 8;58(8):1067–73. [PubMed: 19528167]

57. Li D, Gromov K, Søballe K, Puzas JE, O'Keefe RJ, Awad H, et al. Quantitative mouse model of implant-associated osteomyelitis and the kinetics of microbial growth, osteolysis, and humoral immunity. J Orthop Res. 2008 1;26(1):96–105. [PubMed: 17676625]

58. Jørgensen NP, Meyer R, Dagnæs-Hansen F, Fuursted K. Correction: A Modified Chronic Infection Model for Testing Treatment of Staphylococcus aureus Biofilms on Implants. Vol. 10, PLoS ONE. Public Library of Science; 2015.

59. Funao H, Ishii K, Nagai S, Sasaki A, Hoshikawa T, Aizawa M, et al. Establishment of a real-time, quantitative, and reproducible mouse model of staphylococcus osteomyelitis using bioluminescence imaging. Bäumler AJ, editor. Infect Immun. 2012 2 1;80(2):733–41. [PubMed: 22104103]

60. Ferreira AM, Gentile P, Chiono V, Ciardelli G. Collagen for bone tissue regeneration. Vol. 8, Acta Biomaterialia. 2012. p. 3191–200. [PubMed: 22705634]

61. Zhang D, Wu X, Chen J, Lin K. The development of collagen based composite scaffolds for bone regeneration. Vol. 3, Bioactive Materials. KeAi Communications Co.; 2018. p. 129–38. [PubMed: 29744450]

62. Lang A, Kirchner M, Stefanowski J, Durst M, Weber MC, Pfeiffenberger M, et al. Collagen I-based scaffolds negatively impact fracture healing in a mouse-osteotomy-model although used routinely in research and clinical application. Acta Biomater. 2019 Mar 1;86:171–84. [PubMed: 30616076]

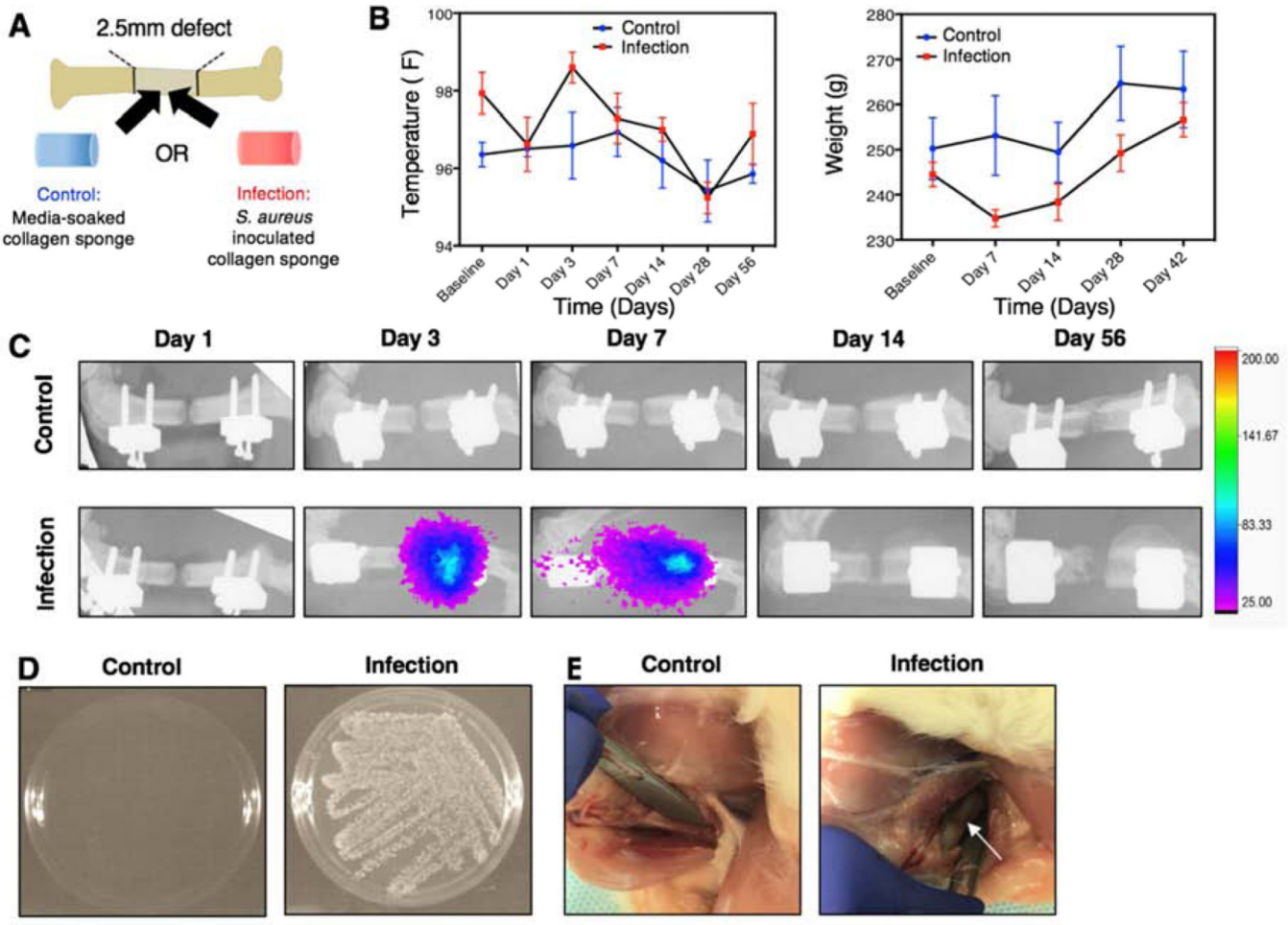

Figure 1. Establishment of a local infection associated with a biomaterial implant.

A) Each animal will receive a 2.5mm segmental bone defect supported by an internal fixation plate. An untreated, media-soaked collagen sponge (control) or a collagen sponge inoculated with *S. aureus* (infection) will be placed into the defect site prior to closure of the surgical site. B) Temperature (left) and weight (right) of the non-infected, control animals and the infection animals. No significant differences between groups overall or at any time point for temperature and weight were observed according to repeated measures 2-way ANOVA. C) Serial bioluminescent and radiograph images taken at Days 1, 3, 7, 14, and 56. Bioluminescent signal appeared in infection animals at Day 3 post-surgery and was present up to Day 7. D) Bacterial culture following wound swab of control and infection animals at the Day 56 endpoint. Bacterial growth is present in the infection group, but not in the control group. E) Representative images of the thighs of euthanized control and infection animals. The white arrow points to gray necrotic soft tissue and purulence around the hardware.

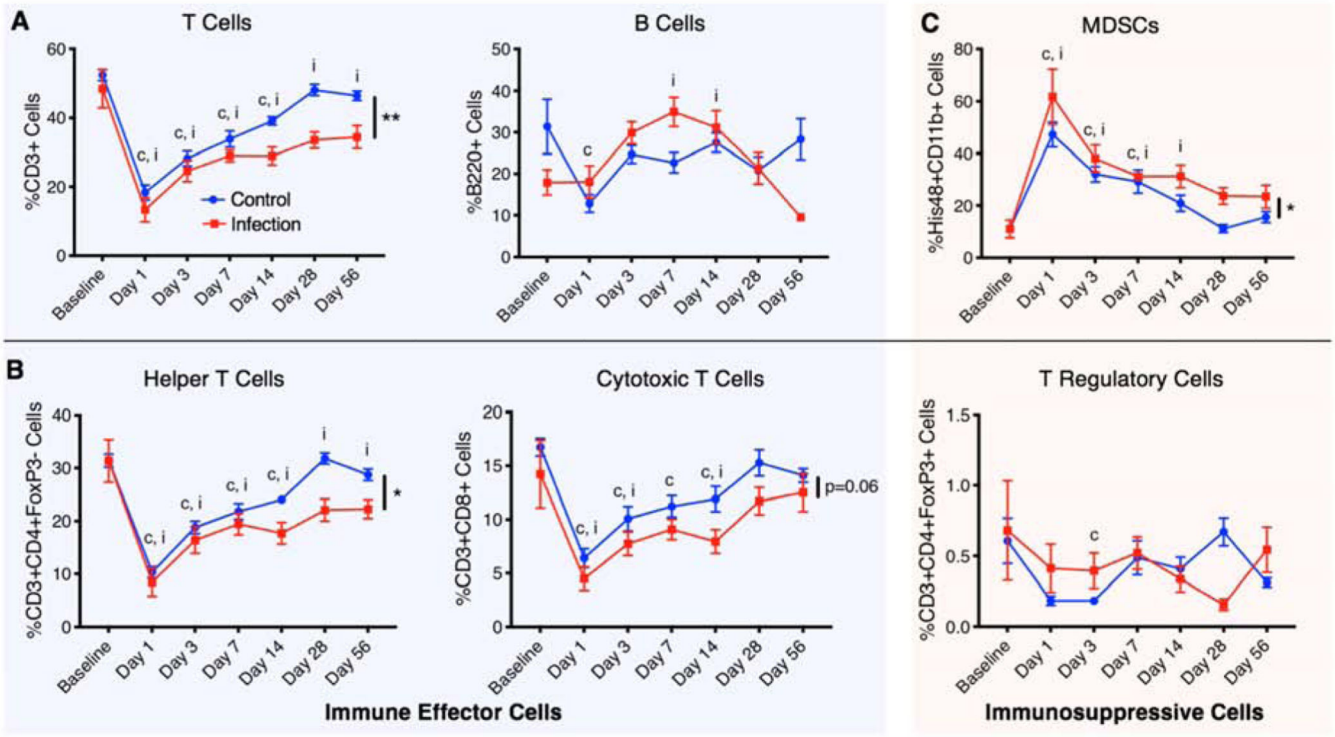

Figure 2. Local infection alters systemic immune cell populations.

Longitudinal analysis of immune cells circulating in the blood including A) lymphocytes (T cells and B cells), B) T cell subsets that include helper T cells, cytotoxic T cells, and T regulatory cells, and C) immunosuppressive MDSCs. These cell types are divided into immune effector cells (T cells, B cells, helper T cells, and cytotoxic T cells) and immunosuppressive cells (MDSCs and T regulatory cells). Overall differences between groups are indicated with a line and the p value or by a ** ($p<0.01$) or * ($p<0.05$). Significant differences ($p<0.05$) from the baseline in the control group and the infection group at specific timepoints are indicated with a “c” and an “i,” respectively. P values were determined by fitting a mixed-effects model (REML) with Sidak’s multiple comparisons test, an analysis similar to repeated measures 2-way ANOVA that can handle missing data points.

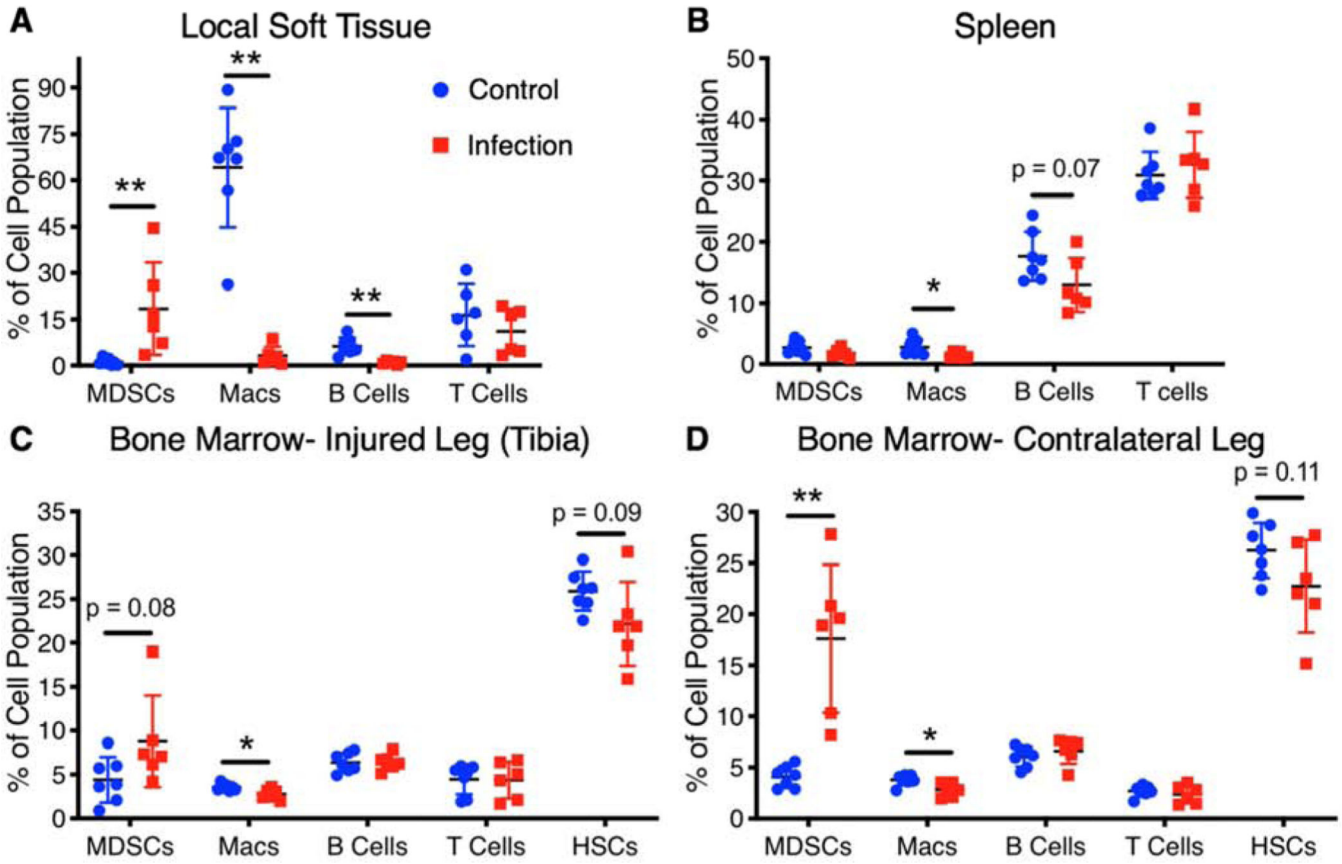

Figure 3. Local infection alters tissue immune cell populations.

Endpoint cellular analyses (Day 56) of tissues including the local soft tissue adjacent to the defect, the spleen, the bone marrow from the contralateral leg, and the bone marrow from the tibia of the injured leg. Differences between groups are indicated by a p value or by * ($p<0.05$) or ** ($p<0.01$). P values obtained using Student's t test or non-parametric Mann-Whitney test when variances are significantly different between groups.

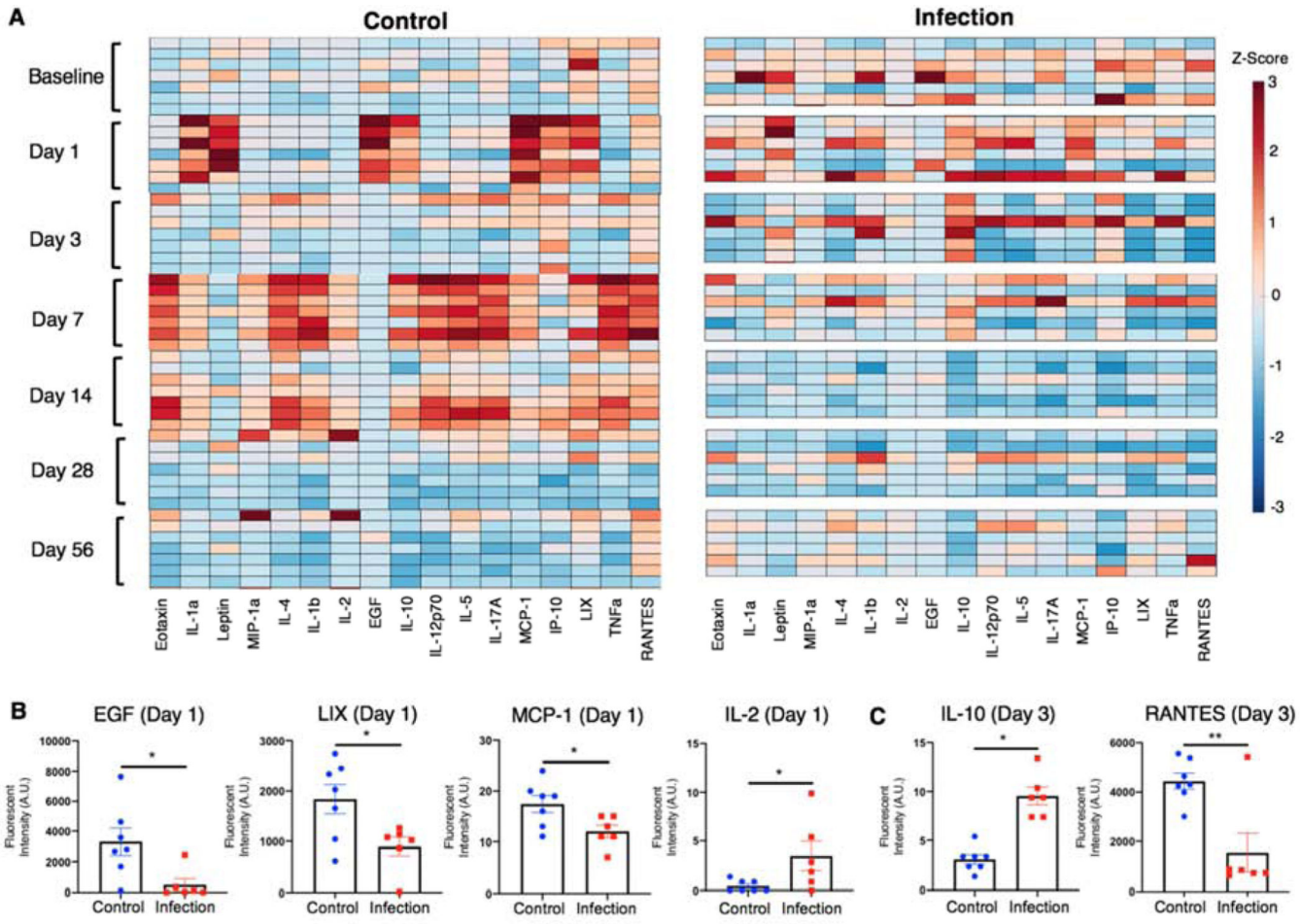

Figure 4. Local infection alters cytokine and chemokine profiles.

A) Heat map of z-scored cytokine levels (each column represents a different cytokine) in the control group (n=7, one n per row) and the infection group (n=6, one n per row) prior to surgery (Baseline) and at Days 1, 3, 7, 14, 28, and 56 post-surgery. Cytokine levels at the two earliest time points that exhibited significant differences between groups are shown for B) Day 1 and C) Day 3. Significance was determined using Student's t-test or with Mann-Whitney test for non-parametric data with $p<0.05$ (*) and $p<0.01$ (**).

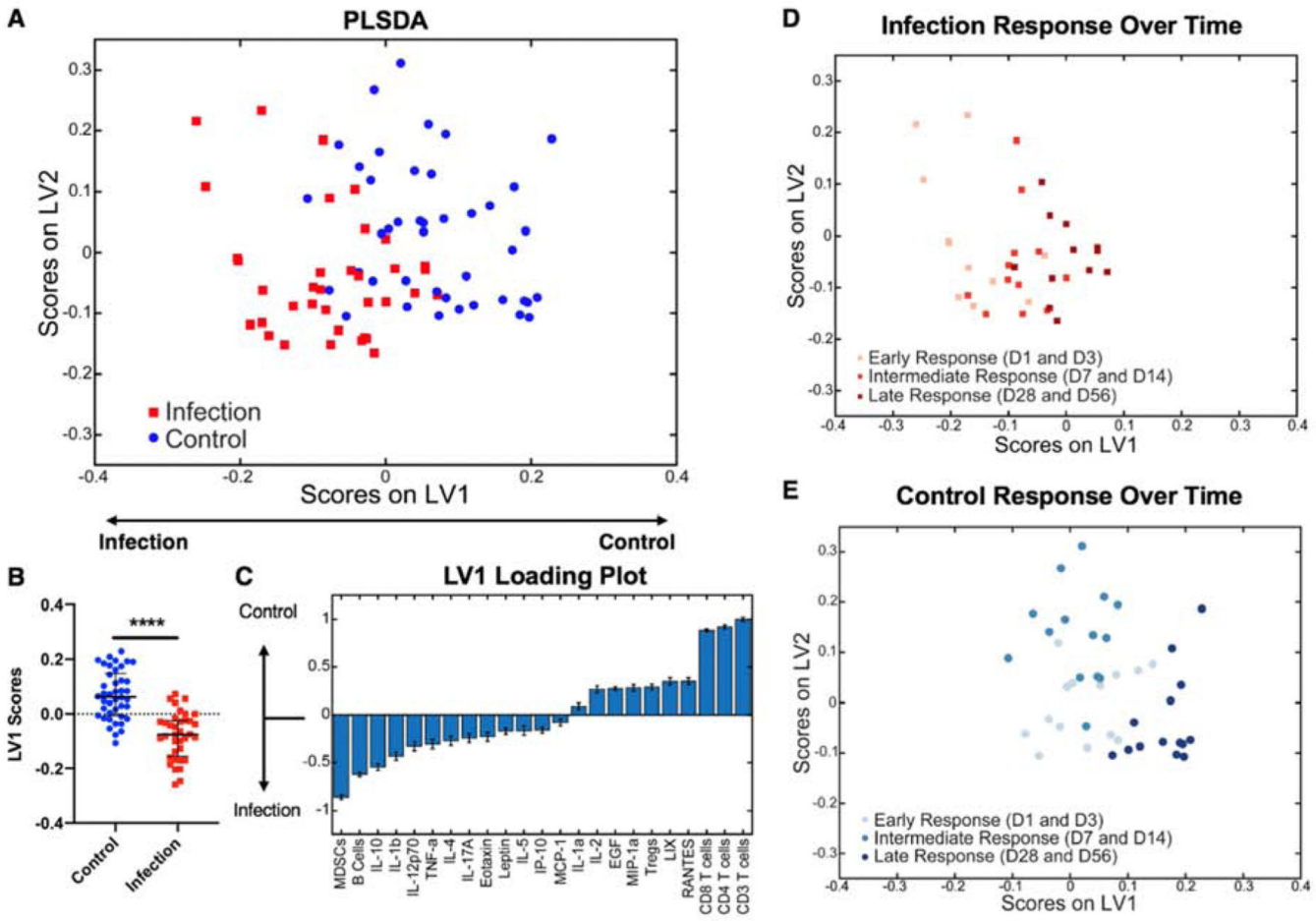

Figure 5. Overall systemic immune characterization.

A) PLSDA plot shows all cytokine levels and cell population values post-surgery for the control group (blue squares) and the infection group (red circles) plotted on latent variable 1 (LV1) and latent variable 2 (LV2) axes. B) Plotting only LV1 scores shows a significant difference ($p<0.001$ (****) according to Student's t-test) between the control and infection groups based on LV1 values. C) The LV1 loading plot shows the top factors that most contributed to positive LV1 scores (right) and the top factors that most contributed to negative LV1 scores (left). Plotting the same datapoints from (A) with only infection data points (D) or only control data points (E) highlights that there is a separation based on response time regardless of infection, including the early response (Day 1 and Day 3), the intermediate response (Day 7 and Day 14), and the late response (Day 28 and Day 56).

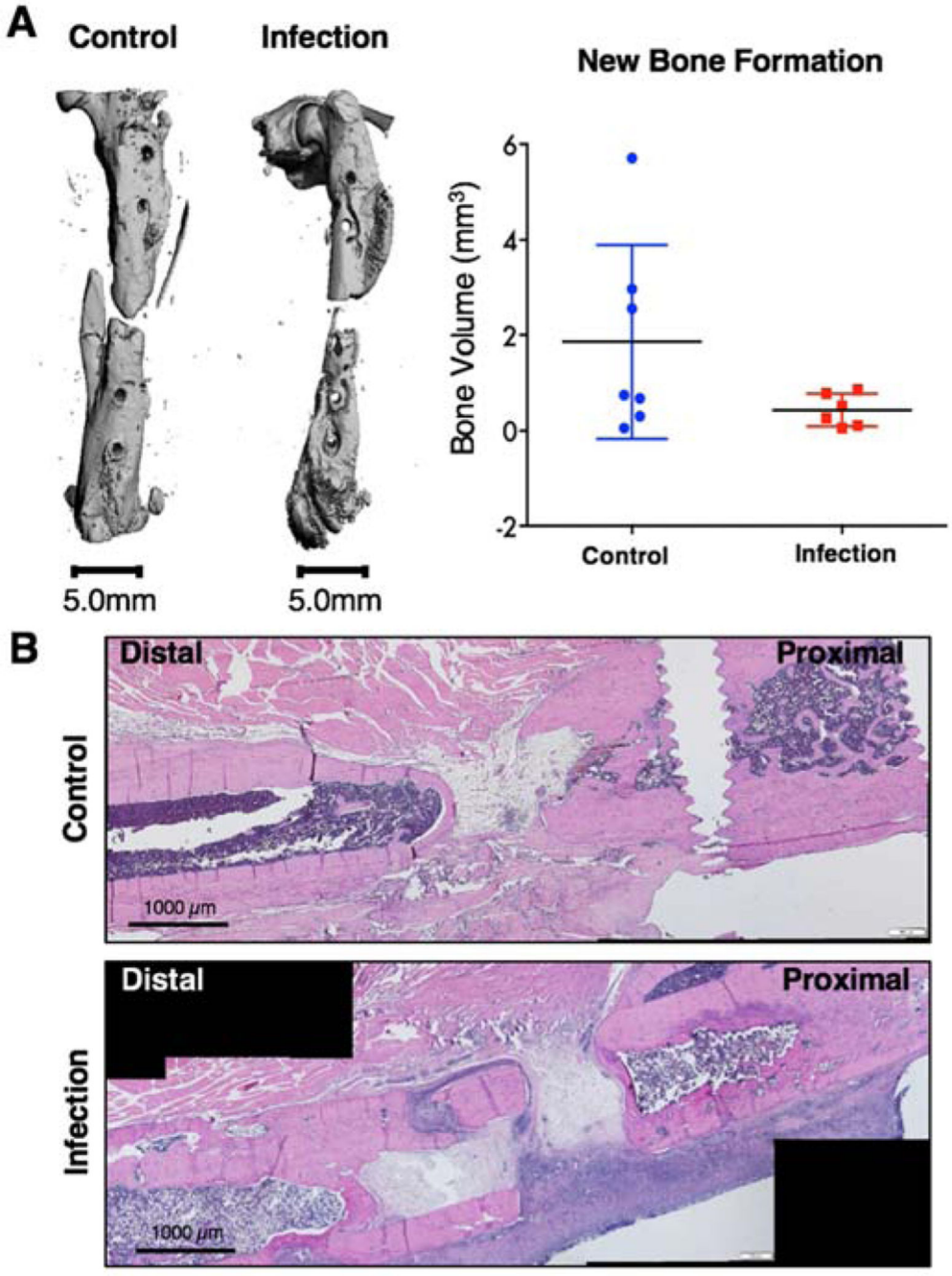

Figure 6. Bone regeneration and histological analysis.

A) Representative endpoint (Day 56) uCT reconstructions (left). Quantification of uCT scans showed no significant differences between the control and infection groups via Mann-Whitney test ($p=0.2343$). B) Representative Hematoxylin &Eosin (H&E) stains of the defect depicting bone formation (pink) and cell presence (nuclei stained purple) within the defect region.